APPLICATION OF THE PREDICTOR-BASED SUBSPACE IDENTIFICATION METHOD TO ROTORCRAFT SYSTEM IDENTIFICATION

Johannes Wartmann, Susanne Seher-Weiss
Johannes.Wartmann@dlr.de, Susanne.Seher-Weiss@dlr.de
German Aerospace Center (DLR), Institute of Flight Systems
Lilienthalplatz 7, 38108 Braunschweig, Germany

ABSTRACT

In this paper, the optimized predictor-based subspace identification (PBSIDopt) method is applied to identify linear models of DLR's research helicopter ACT/FHS and to evaluate its usage to enhance existing physics based models in the future. For this effort, dedicated identification flight test data is used. This paper first describes the well known Maximum Likelihood frequency domain output error method and the applied physical model briefly. Then, the PBSIDopt method is presented and parameters, which influence the identification process, are discussed. Results from both methods using the same flight test data of the ACT/FHS are compared; model accuracy, order and missing dynamics are investigated. Advantages and disadvantages of both methods are evaluated and the applicability of the PBSIDopt method to rotorcraft system identification and its usage to improve the existing physical model structure is discussed.

NOMENCLATURE

$\boldsymbol{A}$, $\boldsymbol{B}$, $\boldsymbol{C}$, $\boldsymbol{D}$	state space matrices
a_x, a_y, a_z	translational accelerations
B, L, M, T, Z	model derivatives (with subscripts)
$\boldsymbol{E}$, $\boldsymbol{U}$, $\boldsymbol{X}$, $\boldsymbol{Y}$	data matrices for system innovations, inputs, states and outputs
$\boldsymbol{e}_k$, $\boldsymbol{u}_k$, $\boldsymbol{x}_k$, $\boldsymbol{y}_k$	discrete time innovation, input, state and output vectors at k-th time step
f, p	future and past window length
J_{RMS}	root mean square error
N	number of measurements
n	model order
n_u, n_y	number of inputs and outputs
p, q, r	roll, pitch and yaw rates
s	Laplace variable
u, v, w	longitudinal, lateral and vertical airspeed components (aircraft-fixed)
$\boldsymbol{u}(t)$, $\boldsymbol{x}(t)$, $\boldsymbol{y}(t)$	continuous time input, state and output vectors
w_{h}	non-physical state for inflow dynamics
x_1, x_2, y_1, y_2	regressive lead-lag system states
$\boldsymbol{y}_{\mathrm{m}}$	measured output (index m)
$\boldsymbol{z}_k$	merged input-output vector at k-th time step
δ_x, δ_y	longitudinal, lateral cyclic pilot controls
δ_p, δ_0	pedal and collective pilot controls
$\boldsymbol{\mathcal{K}}$, $\boldsymbol{\Gamma}$	extended controllability, observability matrix
ν	dynamic inflow
$\boldsymbol{\sigma}^2(\ldots)$	model variance
$\boldsymbol{\tau}$	model parameters
Φ, Θ	roll and pitch attitude angles
$\boldsymbol{\Psi}$	parameters of high order ARX model
ω	frequency
FR	(measured) frequency response
ML	Maximum Likelihood (in frequency domain)
PB, PBSIDopt	optimized predictor-based subspace identification

1. INTRODUCTION

Most current rotorcraft system identification efforts use frequency domain methods to derive linear models. Depending on the model complexity and inclusion of rotor states, the identified models can be accurate for frequencies up to 30 rad/s [1]. As the demands on current control systems increase, the required accuracy of the dynamic models increases, too. To meet these requirements the model's complexity increases and the identification becomes a laborious task. Furthermore, dedicated flight tests have to be performed to generate a suitable data base for the identification and validation tasks, which are essential to arrive at high fidelity models. So both the identification process and the needed flight tests are highly depended on the experimental setup, existing previous knowledge and skilled experimental rotorcraft pilots.

Within the DLR project ALLFlight (Assisted Low Level Flight and Landing on Unprepared Landing Sites [2]), a model-based control system is developed for DLR's research helicopter EC135 ACT/FHS (Active Control Technology/Flying Helicopter Simulator) depicted in figure 1. The ACT/FHS testbed is based on an Eurocopter EC135, a light, twin-engine helicopter with fenestron and bearingless main rotor. Its mechanical controls are replaced by a full-authority fly-by-wire/fly-by-light primary control system, which allows changes of the control inputs applied to the helicopter by an experimental system [3]. Because of the replaced mechanical controls, the dynamic data shown in this paper are not comparable to data from a production EC135 rotorcraft.

Figure 1: DLR's research helicopter ACT/FHS

To design the feedforward and feedback controllers of the model-based control system and later an in-flight simulation, linear models of ACT/FHS have been identified covering the whole flight envelope. The models include rigid body motion, longitudinal and lateral rotor flapping, inflow and regressive lead-lag dynamics and have been identified using the Maximum Likelihood frequency domain method [4–6]. These models have been validated in the time domain, via open loop feedforward controller flight tests [7] and inverse simulation techniques [8]. Both validation methods have shown model deficiencies that are probably caused by missing engine, coning and tail rotor dynamics.

Even if the missing dynamics can be related to physical effects, enhancing the model structure accordingly is not an easy task. In general, submodels are set up based on simplified physical relations to cover the missing dynamics and the original models are enhanced and identified again. If the existing models are complex, like the ACT/FHS models, this task becomes more and more complicated, as connections between different submodels have to be accounted for and their parameters have to be chosen carefully. Furthermore, the submodel structure has to cover the whole flight envelope to simplify the parameter estimation.

Today, state of the art time domain system identification methods like the predictor-based subspace identification method (PBSID) offer the possibility to estimate high order models from open and closed loop data for multiple input and output systems [9, 10]. The PBSID method is numerically stable and applicable to multiple data sets, which is common practice in rotorcraft system identification. The optimized version of the PBSID method (called PBSIDopt) is computationally advantageous and offers even lower estimation errors than PBSID [11, 12]. Thus, the optimized predictor-based subspace identification method seems to be ideal for rotorcraft system identification, but has not yet been tested with flight test data of a full sized manned helicopter [13–16], even if older subspace identification algorithms have been successfully tested with rotorcraft data before [17]. Since the PBSIDopt method automatically estimates states to model the system input-output behavior, no prior knowledge of the physical system structure is needed. Thus, the PBSIDopt method might be used to model missing dynamics of the existing physics based models and might be used to enhance model structure or initial parameter estimates.

In this paper, the classical Maximum Likelihood frequency domain system identification method and the structure of the identified ACT/FHS models are presented in section 2. The PBSIDopt method is presented in section 3; important parameters, model order selection and model reduction are discussed. Models from both methods based on the same identification flight test data are compared in time and frequency domain in section 4. The missing dynamics of the identified Maximum Likelihood model are discussed. Finally this paper is summarized, the advantages and disadvantages of both methods are compared and the application of the PBSIDopt method to enhance the structure of the ACT/FHS models is discussed.

2. ACT/FHS Frequency Domain Identification

2.1. ML Frequency Domain Output Error Method

Assuming that the response $\boldsymbol{y}_\mathrm{m}$ of a dynamic system to an input $\boldsymbol{u}$ has been measured, the goal is to develop a mathematical model that describes the system behavior. For a given linear state space model

$$\dot{\boldsymbol{x}}(t) = \boldsymbol{A}_\mathrm{ML}(\boldsymbol{\tau})\boldsymbol{x}(t) + \boldsymbol{B}_\mathrm{ML}(\boldsymbol{\tau})\boldsymbol{u}(t) \tag{1a}$$

$$\boldsymbol{y}(t) = \boldsymbol{C}_\mathrm{ML}(\boldsymbol{\tau})\boldsymbol{x}(t) + \boldsymbol{D}_\mathrm{ML}(\boldsymbol{\tau})\boldsymbol{u}(t) \tag{1b}$$

the model parameters $\boldsymbol{\tau}$, i.e. the elements of the system matrices $\boldsymbol{A}_\mathrm{ML}$, $\boldsymbol{B}_\mathrm{ML}$, $\boldsymbol{C}_\mathrm{ML}$, $\boldsymbol{D}_\mathrm{ML}$, have to be adjusted so that the simulated model output $\boldsymbol{y}$ matches the measured output $\boldsymbol{y}_\mathrm{m}$ for the same input history $\boldsymbol{u}$.

The discretely sampled time dependent variable

$$\boldsymbol{x}_k = \boldsymbol{x}(k\Delta t)\,, \quad k = 0, \ldots, N-1 \tag{2}$$

with the sampling time interval Δt is transformed into a frequency dependent variable using the Fourier transform

$$\boldsymbol{x}(\omega_k) = \frac{1}{N}\sum_{k=0}^{N-1} \boldsymbol{x}_k \mathrm{e}^{-\mathrm{j}\omega_k k\Delta t} \tag{3a}$$

$$\omega_k = k \cdot 2\pi / t_N \;\text{ with }\; t_N = (N-1)\Delta t\,. \tag{3b}$$

The variables $\dot{\boldsymbol{x}}$, $\boldsymbol{x}$, $\boldsymbol{u}$, $\boldsymbol{y}$ of the linear model from equation (1) and the measured output $\boldsymbol{y}_{\mathrm{m}}$ are transformed into the frequency domain in this way. One has to note that the state variables do not always fulfill the condition of periodicity. According to [18], the Fourier transform of $\dot{\boldsymbol{x}}$ is in this case approximately given by

$$\dot{\boldsymbol{x}}(\omega) = \mathrm{j}\omega\boldsymbol{x}(\omega) - \boldsymbol{b}_p\bar{\boldsymbol{u}}(\omega) \tag{4a}$$

$$\boldsymbol{b}_p = \frac{1}{2t_N}\left[(\boldsymbol{x}_{N-1} + \boldsymbol{x}_N) - (\boldsymbol{x}_{-1} + \boldsymbol{x}_0)\right] \tag{4b}$$

$$\bar{\boldsymbol{u}}(\omega) = \mathrm{e}^{\frac{1}{2}\mathrm{j}\omega\Delta t} \tag{4c}$$

which requires two additional data points $\boldsymbol{x}_{-1}$ and $\boldsymbol{x}_N$ not used in equation (3). The model equations in the frequency domain are therefore

$$\mathrm{j}\omega\boldsymbol{x}(\omega) = \boldsymbol{A}_{\mathrm{ML}}(\boldsymbol{\tau})\boldsymbol{x}(\omega) + \boldsymbol{B}_{\mathrm{ML}}(\boldsymbol{\tau})\boldsymbol{u}(\omega) + \boldsymbol{b}_p\bar{\boldsymbol{u}}(\omega) \tag{5a}$$

$$\boldsymbol{y}(\omega) = \boldsymbol{C}_{\mathrm{ML}}(\boldsymbol{\tau})\boldsymbol{x}(\omega) + \boldsymbol{D}_{\mathrm{ML}}(\boldsymbol{\tau})\boldsymbol{u}(\omega). \tag{5b}$$

The Maximum Likelihood (ML) method in the frequency domain minimizes

$$\min_{\boldsymbol{\tau}} \left(\prod_{i=1}^{n_y} \boldsymbol{\sigma}^2\left(\boldsymbol{y}_{\mathrm{m},i} - \boldsymbol{y}_i(\boldsymbol{\tau})\right) \right) \text{ with} \tag{6}$$

$$\boldsymbol{\sigma}^2\left(\boldsymbol{y}_{\mathrm{m},i} - \boldsymbol{y}_i(\boldsymbol{\tau})\right) = \frac{1}{N}\sum_{k=0}^{N-1} \left(\boldsymbol{y}_{\mathrm{m},i}(\omega_k) - \boldsymbol{y}_i(\omega_k)\right)^* \left(\boldsymbol{y}_{\mathrm{m},i}(\omega_k) - \boldsymbol{y}_i(\omega_k)\right) \tag{7}$$

where $()^*$ denotes the conjugate transpose of a complex value, n_y the number of system outputs and $\boldsymbol{\sigma}^2(\ldots)$ the model variance. The minimization problem from equation (6) is solved using e.g. a Gauss-Newton optimization method.

Parameter estimation in the frequency domain has the advantage that it is possible to significantly reduce the amount of data to be evaluated by restricting the evaluation to the frequency range of interest. The higher frequencies can often be omitted safely because they correspond to measurement noise and negligible higher order dynamics.

When the lowest frequency ($\omega = 0$) is omitted, the estimation of bias parameters is suppressed, thus leading to much fewer unknown parameters, especially when several time intervals are evaluated together. One possibility to include the estimation of bias parameters is to first identify the system parameters using frequency domain identification and afterwards to only identify the bias parameters using time domain identification with the matrices $\boldsymbol{A}_{\mathrm{ML}}$, $\boldsymbol{B}_{\mathrm{ML}}$, $\boldsymbol{C}_{\mathrm{ML}}$, $\boldsymbol{D}_{\mathrm{ML}}$ fixed at the identified values. As the model equation (5) are algebraic, no integration is necessary to calculate the output variables. This makes frequency domain models very suitable for unstable systems.

2.2. Model Structure for ACT/FHS Identification

The quasi-steady formulation of the helicopter dynamics by a classical six degree of freedom rigid body model is valid only up to about 10 rad/s. To arrive at high fidelity models valid up to 30 rad/s, as is required for model following control, the higher order effects of rotor flapping, dynamic inflow and rotor-lead-lag have to be accounted for. As the identified models have to be invertible, only linear models are used here. For the ACT/FHS identification, implicit modeling of flapping and inflow dynamics is used. The utilized equations are derived briefly in the following paragraphs. More detailed information about the effect of including the different rotor states in the system identification model can be found in [4–6].

2.2.1. Flapping

To account for flapping, the first order on-axis response for the roll rate

$$\dot{p} = L_p p + L_{\delta_y}\delta_y \tag{8}$$

is replaced by

$$\dot{p} = L_b b \tag{9}$$

$$\tau_f\dot{b} = -\tau_f p - b + B_{\delta_y}\delta_y \tag{10}$$

where b is the lateral flapping angle and L_b the corresponding derivative. Equation (9) makes the roll acceleration proportional to the lateral flapping angle. Equation (10) is a first order rotor equation with the lateral flapping time constant τ_f and the control derivative B_{δ_y}. Similar equations hold for the longitudinal flapping coupled to pitch rate.

The model is reformulated by differentiating equation (9) and inserting equation (10) as well as the expression for b from equation (9), which results in the implicit formulation for flapping with modified derivatives

$$\begin{aligned}\ddot{p} &= -L_b p - \frac{1}{\tau_f}\dot{p} + L_b\frac{B_{\delta_y}}{\tau_f}\delta_y \\ &= \hat{L}_p p + \hat{L}_{\dot{p}}\dot{p} + \hat{L}_{\delta_y}\delta_y\ .\end{aligned} \tag{11}$$

The corresponding equation for pitch rate is

$$\ddot{q} = \hat{M}_q q + \hat{M}_{\dot{q}}\dot{q} + \hat{M}_{\delta_x}\delta_x\ . \tag{12}$$

The incorporation of the flapping motion using this model thus leads to $\dot{p}$ and $\dot{q}$ as two additional state variables, resulting in an eight degree of freedom model with ten states.

2.2.2. Dynamic Inflow

The dynamic equations for the helicopter's vertical velocity w and inflow ν for a rigid rotor (neglecting coning) are

$$\dot{w} = Z_w w + Z_{\dot{\nu}}\dot{\nu} + Z_\nu\nu \tag{13}$$

$$\dot{\nu} = T_w w + T_\nu\nu + T_{\delta_0}\delta_0\ . \tag{14}$$

Here, the thrust equation (14) is derived from the principle of linear momentum. Inserting equation (14) into equation (13) eliminates $\dot{\nu}$ and leads to

$$\begin{aligned}\dot{w} &= (Z_w + Z_{\dot{\nu}} T_w) w + (Z_{\dot{\nu}} T_\nu + Z_\nu)\nu + Z_{\dot{\nu}} T_{\delta_0} \delta_0 \\ &= \bar{Z}_w w + \bar{Z}_\nu \nu + \bar{Z}_{\delta_0} \delta_0 \ .\end{aligned} \tag{15}$$

Solving for ν yields

$$\nu = \frac{1}{\bar{Z}_\nu}(\dot{w} - \bar{Z}_w w - \bar{Z}_{\delta_0}\delta_0) \ . \tag{16}$$

Differentiating equation (15) with respect to time and inserting the expressions for $\dot{\nu}$ and ν from equation (14) and equation (16) gives the implicit formulation for dynamic inflow

$$\begin{aligned}\ddot{w} &= (\bar{Z}_\nu T_w - T_\nu \bar{Z}_w) w + (\bar{Z}_w + T_\nu)\dot{w} \\ &\quad + (\bar{Z}_\nu T_{\delta_0} - T_\nu \bar{Z}_{\delta_0})\delta_0 + \bar{Z}_{\delta_0}\dot{\delta}_0 \\ &= \hat{Z}_w w + \hat{Z}_{\dot{w}}\dot{w} + \hat{Z}_{\delta_0}\delta_0 + \hat{Z}_{\dot{\delta}_0}\dot{\delta}_0 \ .\end{aligned} \tag{17}$$

This differential equation for $\ddot{w}$ has both δ_0 and $\dot{\delta}_0$ as inputs. Alternatively, δ_0 can be added to the model as a state variable, which then leaves $\dot{\delta}_0$ as the only vertical control input. This approach is equivalent to the one suggested by [19] where the dynamic inflow is approximated by a first-order lead-lag filter on the collective term in the vertical axis.

2.2.3. Regressive Lead-Lag

Simple physical models for the regressive lead-lag dynamics, such as those for the flapping dynamics, are not available. Therefore, a modal approach is usually taken, where a second order transfer function is appended to the pitch and roll rate responses without regressive lead-lag dynamics due to longitudinal and lateral input respectively [1]

$$\left(\frac{q}{\delta_x}\right)_{\text{(with lead-lag)}} = \left(\frac{q}{\delta_x}\right)_{\text{(without lead-lag)}} \frac{[\zeta_{xq}, \omega_{xq}]}{[\zeta_{ll}, \omega_{ll}]} \tag{18}$$

Here, $[\zeta, \omega]$ denotes a complex root with damping ζ and natural frequency ω and the index ll stands for lead-lag mode. Four of these second order transfer functions are necessary to model the lead-lag effect on pitch and roll rate for cyclic inputs ($\delta_x \rightarrow q,\ \delta_x \rightarrow p,\ \delta_y \rightarrow p,\ \delta_y \rightarrow q$). All transfer functions have a common denominator due to same underlying physical phenomenon.

The transfer functions of the regressive lead-lag dynamics are formulated to have a static gain of 1 such that the low-frequency part of the transfer function (derived from the model without lead-lag) is left unchanged when the lead-lag is added. Regarding the pitch rate due to longitudinal cyclic input $\delta_x \rightarrow q$, the transfer function thus is

$$\begin{aligned}\frac{\delta_{xq}}{\delta_x} &= \frac{(s^2 + 2\zeta_{xq}\omega_{xq}s + \omega_{xq}^2)/\omega_{xq}^2}{(s^2 + 2\zeta_{ll}\omega_{ll}s + \omega_{ll}^2)/\omega_{ll}^2} \\ &= \frac{\omega_{ll}^2}{\omega_{xq}^2}\left(1 + \frac{2(\zeta_{xq}\omega_{xq} - \zeta_{ll}\omega_{ll})s + (\omega_{xq}^2 - \omega_{ll}^2)}{s^2 + 2\zeta_{ll}\omega_{ll}s + \omega_{ll}^2}\right) \ .\end{aligned} \tag{19}$$

For use in a state space identification model, the transfer functions have to be transformed into differential equations. An auxiliary variable x_{ll} is introduced that is defined by

$$\frac{x_{ll}}{\delta_x} = s^2 + 2\zeta_{ll}\omega_{ll}s + \omega_{ll}^2 \tag{20}$$

and thus has the differential equation

$$\ddot{x}_{ll} + 2\zeta_{ll}\omega_{ll}\dot{x}_{ll} + \omega_{ll}^2 x_{ll} = \delta_x \ . \tag{21}$$

This second order differential equation is transformed into two first order differential equations by introducing $x_1 = x_{ll}$ and $x_2 = \dot{x}_{ll}$

$$\dot{x}_1 = x_2 \tag{22a}$$

$$\dot{x}_2 = -\omega_{ll}^2 x_1 - 2\zeta_{ll}\omega_{ll}x_2 + \delta_x \ . \tag{22b}$$

The output equation for δ_{xq} can be derived from equation (19) as

$$\begin{aligned}\delta_{xq} &= \frac{\omega_{ll}^2}{\omega_{xq}^2}(\omega_{xq}^2 - \omega_{ll}^2)x_1 \\ &\quad + 2\frac{\omega_{ll}^2}{\omega_{xq}^2}(\zeta_{xq}\omega_{xq} - \zeta_{ll}\omega_{ll})x_2 + \frac{\omega_{ll}^2}{\omega_{xq}^2}\delta_x \ .\end{aligned} \tag{23}$$

This last equation describes how the original control input δ_x is to be replaced in the differential equation for $\dot{q}$. Equation (23) contains two terms that are to become part of the system matrix $\boldsymbol{A}_{\mathrm{ML}}$ and one that belongs to the control matrix $\boldsymbol{B}_{\mathrm{ML}}$.

Regarding the structure of the transfer function listed in equation (19), it can be seen that two differential equations of the form in equation (22) with the same denominator are needed for each control input (δ_x, δ_y). This hybrid model approach does not cover the physics (and thus rotor states) of the regressive lead-lag dynamics, but represents the frequency responses of $\dot{p}$, $\dot{q}$ and their integrals accurately.

2.2.4. Overall ACT/FHS Model Structure

The overall ACT/FHS model used for system identification contains 16 states, namely eight for the rigid-body motion (u, v, w, p, q, r, Φ, Θ), two for implicit flapping ($\dot{p}$, $\dot{q}$), two for implicit dynamic inflow ($\dot{w}$, δ_0) and four for lead-lag (x_1, x_2, y_1, y_2). The system identification was performed over a frequency range of 0.5-20 rad/s.

After the system identification process, the physical state $\dot{w}$ and the derivative of the collective control $\dot{\delta}_0$ are replaced by a non-physical state w_{h} and the collective control δ_0, because this formulations is advantageous for the later model simulation, for more details see [20]. Thus, the Maximum Likelihood model used for comparison contains 15 states

$$\boldsymbol{x}(t) = (u\ \ v\ \ w\ \ p\ \ q\ \ r\ \ w_{\mathrm{h}}\ \ \dot{p}\ \ \dot{q}\ \ \Phi\ \ \Theta\ \ x_1\ \ x_2\ \ y_1\ \ y_2)^T \tag{24}$$

and the four helicopter controls for longitudinal and lateral cyclic δ_x and δ_y, pedal δ_p and collective control δ_0 as inputs

$$\boldsymbol{u}(t) = \begin{pmatrix}\delta_x & \delta_y & \delta_p & \delta_0\end{pmatrix}^T \ . \tag{25}$$

During system identification process 15 outputs $\boldsymbol{y}(t)$ including the translational accelerations a_x, a_y and a_z are matched

(26)
$$\boldsymbol{y}(t) = (u \;\; v \;\; w \;\; p \;\; q \;\; r \;\; \dot{p} \;\; \dot{q} \;\; \dot{r} \;\; \Phi \;\; \Theta \;\; a_x \;\; a_y \;\; a_z \;\; \dot{a}_z)^T .$$

The angular accelerations $\dot{p}$, $\dot{q}$, $\dot{r}$ and the derivative of the vertical acceleration $\dot{a}_z$ are not measured directly, but are obtained by a suitable numerical differentiation. Adding them as output variables, improves the identifiability of the equivalent flapping and inflow dynamics respectively.

2.3. System Identification Database

To support the in-flight simulation efforts, models for the EC135 ACT/FHS research helicopter that cover the whole envelope from hover up to 120 knots forward flight had to be identified. Dedicated flight tests for this purpose, consisting of frequency sweeps and multi-step inputs in all four controls, were performed at five reference flight conditions (hover, 30 knots, 60 knots, 90 knots, 120 knots). During the flight tests, the pilots were instructed to use only uncorrelated, pulse-type inputs on the secondary controls to avoid cross-correlation between the control inputs. The multi-step inputs were computer generated, which allows for relatively sharp input signals and avoids correlation problems.

The frequency domain identification was performed using two pilot generated frequency sweeps per control input (longitudinal and lateral cyclic, collective and pedal input). For validation of the identified models in the time domain, the multi-step input maneuvers were used.

3. ACT/FHS System Identification using the PBSIDopt Method

3.1. The PBSIDopt Method

The PBSIDopt method estimates a discrete linear time invariant state space model in innovation form as described in [21]

(27a) $$\boldsymbol{x}_{k+1} = \boldsymbol{A}\boldsymbol{x}_k + \boldsymbol{B}\boldsymbol{u}_k + \boldsymbol{K}\boldsymbol{e}_k$$
(27b) $$\boldsymbol{y}_k = \boldsymbol{C}\boldsymbol{x}_k + \boldsymbol{D}\boldsymbol{u}_k + \boldsymbol{e}_k$$

from a finite set of data points $\boldsymbol{u}_k$ and $\boldsymbol{y}_k$, $k = 1, \ldots N$. Here, $\boldsymbol{u}_k \in \mathbb{R}_{n_u}$ are the system inputs, $\boldsymbol{x}_k \in \mathbb{R}_n$ the system states and $\boldsymbol{e}_k$, $\boldsymbol{y}_k \in \mathbb{R}_{n_y}$ the system innovations and the outputs respectively. The model order n is equal to the number of states $\boldsymbol{x}_k$.

The system matrices from equation (27) correspond to the system matrices of a discrete process form state space system

(28a) $$\tilde{\boldsymbol{x}}_{k+1} = \boldsymbol{A}\tilde{\boldsymbol{x}}_k + \boldsymbol{B}\boldsymbol{u}_k + \boldsymbol{w}_k$$
(28b) $$\boldsymbol{y}_k = \boldsymbol{C}\tilde{\boldsymbol{x}}_k + \boldsymbol{D}\boldsymbol{u}_k + \boldsymbol{v}_k$$

with process noise $\boldsymbol{w}_k$, measurement noise $\boldsymbol{v}_k$ and a different state vector $\tilde{\boldsymbol{x}}_k$ compared to equation (27).

The innovation form state space system from equation (27) is transformed into the predictor form assuming there is no direct feedthrough, i.e. $\boldsymbol{D} = \boldsymbol{0}$

(29a) $$\boldsymbol{x}_{k+1} = \boldsymbol{A}_K\boldsymbol{x}_k + \boldsymbol{B}_K\boldsymbol{z}_k$$
(29b) $$\boldsymbol{y}_k = \boldsymbol{C}\boldsymbol{x}_k + \boldsymbol{e}_k$$

with

(30a) $$\boldsymbol{A}_K = \boldsymbol{A} - \boldsymbol{K}\boldsymbol{C}\,, \quad \boldsymbol{B}_K = \begin{pmatrix}\boldsymbol{B} & \boldsymbol{K}\end{pmatrix} \text{ and}$$
(30b) $$\boldsymbol{z}_k = \begin{pmatrix}\boldsymbol{u}_k & \boldsymbol{y}_k\end{pmatrix}^T .$$

From the physical point of view only forces and moments (corresponding to translational and rotational accelerations) can be changed instantly. Therefore, the assumption $\boldsymbol{D} = \boldsymbol{0}$ is only valid for rotorcraft system identification using velocities, rates and angles as outputs. Nevertheless, the assumption $\boldsymbol{D} = \boldsymbol{0}$ in the following algorithm can be modified easily to account for the direct feedthrough $\boldsymbol{D}$ [15]. Since the system matrix $\boldsymbol{A}_K$ is stable, this formulation is applicable to the identification of unstable systems like rotorcraft.

In the first PBSIDopt step the states $\boldsymbol{x}$, here called predictors due to the predictor form in equation (29), are estimated. The predictors $\boldsymbol{x}_i$ (with $i = 3, \ldots N$) at the third up to the N-th time step are defined by

(31)
$$\begin{aligned}\boldsymbol{x}_3 &= \boldsymbol{A}_K\boldsymbol{x}_2 + \boldsymbol{B}_K\boldsymbol{z}_2 \\ &= \boldsymbol{A}_K^2\boldsymbol{x}_1 + \begin{pmatrix}\boldsymbol{A}_K\boldsymbol{B}_K & \boldsymbol{B}_K\end{pmatrix}\begin{pmatrix}\boldsymbol{z}_1 \\ \boldsymbol{z}_2\end{pmatrix} \\ &\vdots \\ \boldsymbol{x}_N &= \boldsymbol{A}_K^2\boldsymbol{x}_1 + \begin{pmatrix}\boldsymbol{A}_K^{N-1}\boldsymbol{B}_K & \ldots & \boldsymbol{B}_K\end{pmatrix}\begin{pmatrix}\boldsymbol{z}_1 \\ \vdots \\ \boldsymbol{z}_{N-1}\end{pmatrix} .\end{aligned}$$

The corresponding system outputs for the second up to the N-th time step are given by

(32)
$$\begin{aligned}\boldsymbol{y}_2 &= \boldsymbol{C}\boldsymbol{A}_K^2\boldsymbol{x}_1 + \boldsymbol{C}\boldsymbol{\mathcal{K}}^N\begin{pmatrix}\boldsymbol{0} \\ \vdots \\ \boldsymbol{z}_1 \\ \boldsymbol{z}_2\end{pmatrix} + \boldsymbol{e}_2 \\ &\vdots \\ \boldsymbol{y}_N &= \boldsymbol{C}\boldsymbol{A}_K^2\boldsymbol{x}_1 + \boldsymbol{C}\boldsymbol{\mathcal{K}}^N\begin{pmatrix}\boldsymbol{z}_1 \\ \vdots \\ \boldsymbol{z}_{N-1}\end{pmatrix} + \boldsymbol{e}_N\end{aligned}$$

with the extended controllability matrix

(33) $$\boldsymbol{\mathcal{K}}^N = \begin{pmatrix}\boldsymbol{A}_K^{N-1}\boldsymbol{B}_K & \ldots & \boldsymbol{B}_K\end{pmatrix} .$$

In order to describe the system outputs from the p+1-th to the N-th time step, the following data matrices for the system output and innovation are defined

$$\boldsymbol{Y}_{p+1} = \begin{pmatrix} \boldsymbol{y}_{p+1} & \boldsymbol{y}_{p+2} & \dots & \boldsymbol{y}_N \end{pmatrix} \tag{34a}$$

$$\boldsymbol{E}_{p+1} = \begin{pmatrix} \boldsymbol{e}_{p+1} & \boldsymbol{e}_{p+2} & \dots & \boldsymbol{e}_N \end{pmatrix}. \tag{34b}$$

The predictor form model input vector $\boldsymbol{z}$ is collected in the Hankel matrix

$$\boldsymbol{Z}_p = \begin{pmatrix} \boldsymbol{z}_1 & \boldsymbol{z}_2 & \dots & \boldsymbol{z}_{N-p-1} \\ \boldsymbol{z}_2 & \boldsymbol{z}_3 & \dots & \boldsymbol{z}_{N-p-2} \\ \vdots & \vdots & \dots & \vdots \\ \boldsymbol{z}_p & \boldsymbol{z}_{p+1} & \dots & \boldsymbol{z}_{N-1} \end{pmatrix}. \tag{35}$$

The integer variable p is called past window length or past horizon in the subspace identification. Together with the model order n and the future window length f, which is introduced later in equation (39), this parameter has a huge impact on the identification results.

Assuming the past window length p is large and $\boldsymbol{A}_K$ is stable, the term $\boldsymbol{A}_K^2 \boldsymbol{x}_1$ in equation (32) can be neglected and the p+1-th to N-th system outputs and states are approximated using the data matrices $\boldsymbol{Y}_{p+1}$, $\boldsymbol{E}_{p+1}$ and $\boldsymbol{Z}_p$

$$\boldsymbol{Y}_{p+1} \approx \boldsymbol{C}\boldsymbol{\mathcal{K}}^p \boldsymbol{Z}_p + \boldsymbol{E}_{p+1} \tag{36a}$$

$$\boldsymbol{X}_{p+1} \approx \boldsymbol{\mathcal{K}}^p \boldsymbol{Z}_p. \tag{36b}$$

An estimate of $\boldsymbol{C}\boldsymbol{\mathcal{K}}^p \approx \boldsymbol{\Psi}$ is obtained solving the least squares problem

$$\min_{\boldsymbol{\Psi}} \left\| \boldsymbol{Y}_{p+1} - \boldsymbol{\Psi} \boldsymbol{Z}_p \right\|. \tag{37}$$

Recalling equation (33), the coefficient matrix $\boldsymbol{\Psi}$ is an estimate of

$$\boldsymbol{\Psi} = \begin{pmatrix} \boldsymbol{\Psi}_p \dots \boldsymbol{\Psi}_1 \end{pmatrix} \approx \begin{pmatrix} \boldsymbol{C}\boldsymbol{A}_K^{p-1}\boldsymbol{B}_K & \dots & \boldsymbol{C}\boldsymbol{B}_K \end{pmatrix} \tag{38}$$

and is used to set up the product of the extended observability matrix $\boldsymbol{\Gamma}^f$ and the extended controllability matrix $\boldsymbol{\mathcal{K}}^p$

$$\boldsymbol{\Gamma}^f \boldsymbol{\mathcal{K}}^p = \begin{pmatrix} \boldsymbol{C}\boldsymbol{A}_K^{p-1}\boldsymbol{B}_K & \dots & \boldsymbol{C}\boldsymbol{B}_K \\ \boldsymbol{0} & \dots & \boldsymbol{C}\boldsymbol{A}_K\boldsymbol{B}_K \\ \vdots & \vdots & \vdots \\ \boldsymbol{0} & \dots & \boldsymbol{C}\boldsymbol{A}_K^{f-1}\boldsymbol{B}_K \end{pmatrix} \tag{39}$$

with the future window length f.

Using the singular value decomposition

$$\boldsymbol{\Gamma}^f \boldsymbol{\mathcal{K}}^p \boldsymbol{Z}_p = \boldsymbol{U}\boldsymbol{S}\boldsymbol{V}^T = \begin{pmatrix} \boldsymbol{U}_n & \tilde{\boldsymbol{U}} \end{pmatrix} \begin{pmatrix} \boldsymbol{S}_n & \boldsymbol{0} \\ \boldsymbol{0} & \tilde{\boldsymbol{S}} \end{pmatrix} \begin{pmatrix} \boldsymbol{V}_n^T \\ \tilde{\boldsymbol{V}}^T \end{pmatrix}, \tag{40}$$

the predictor sequence $\boldsymbol{X}_{p+1}$ is calculated through

$$\boldsymbol{X}_{p+1} \approx \boldsymbol{S}_n^{\frac{1}{2}} \boldsymbol{V}_n^T \tag{41}$$

since

$$\boldsymbol{\Gamma}^f \boldsymbol{X}_{p+1} \approx \boldsymbol{\Gamma}^f \boldsymbol{\mathcal{K}}^p \boldsymbol{Z}_p. \tag{42}$$

The neglect of the smaller singular values $\tilde{\boldsymbol{S}} \approx \boldsymbol{0}$ in the predictor sequence reconstruction can be interpreted as a model reduction step to the selected model order n. An analysis of the singular values in $\boldsymbol{S}$ is often used to select an appropriate model order n.

Alternatively, the estimation of a high order predictor sequence can be used to cover high order dynamics in the model to be identified and the final model can be reduced afterwards using other model reduction techniques. This can be used for example to gain models valid in a frequency range of interest for controller design applications only.

In the second PBSIDopt step, the system innovation $\boldsymbol{e}_k$ and the system matrices of the innovation form in equation (27) are estimated. Since the input, output and estimated state sequence is used in this step, it is referred to as state sequence approach in subspace identification.

Using equation (27) and $\boldsymbol{D} = \boldsymbol{0}$, the output matrix $\boldsymbol{C}$ can be estimated solving the least squares problem

$$\min_{\boldsymbol{C}} \left\| \boldsymbol{Y}_{p+1} - \boldsymbol{C}\boldsymbol{X}_{p+1} \right\| \tag{43}$$

and the system innovations are calculated by

$$\boldsymbol{E}_{p+1} = \boldsymbol{Y}_{p+1} - \boldsymbol{C}\boldsymbol{X}_{p+1}. \tag{44}$$

Considering that the $k+1$-th state is calculated from $\boldsymbol{x}_k$, $\boldsymbol{u}_k$ and $\boldsymbol{e}_k$, the data matrices $\boldsymbol{X}_{p+1}$ and $\boldsymbol{E}_{p+1}$ are split up and an input data matrix is defined. MATLAB® notation is used for simplicity here:

$$\boldsymbol{X}_{k+1} = \boldsymbol{X}_{p+1}(:,2{:}N) \tag{45a}$$

$$\boldsymbol{X}_k = \boldsymbol{X}_{p+1}(:,1{:}N\text{-}1) \tag{45b}$$

$$\boldsymbol{E}_k = \boldsymbol{E}_{p+1}(:,1{:}N\text{-}1) \tag{45c}$$

$$\boldsymbol{U}_k = \begin{pmatrix} \boldsymbol{u}_p & \boldsymbol{u}_{p+1} & \dots & \boldsymbol{u}_{N-1} \end{pmatrix}. \tag{45d}$$

The matrices $\boldsymbol{A}$, $\boldsymbol{B}$ and $\boldsymbol{K}$ are estimated solving

$$\min_{\boldsymbol{A},\boldsymbol{B},\boldsymbol{K}} \left\| \boldsymbol{X}_{k+1} - \boldsymbol{A}\boldsymbol{X}_k - \boldsymbol{B}\boldsymbol{U}_k - \boldsymbol{K}\boldsymbol{E}_k \right\|. \tag{46}$$

The estimated discrete linear model matrices $\boldsymbol{A}$, $\boldsymbol{B}$ and $\boldsymbol{C}$ are used to set up the process model in equation (28). The inverse bilinear or any other discrete to continuous transformation can then be used to calculate the continuous time model.

Flight tests for rotorcraft system identification, as described in subsection 2.3, usually consist of different datasets from a number of experiments. To handle j different datasets, the data matrices $\boldsymbol{Y}_{p+1}$ and $\boldsymbol{Z}_p$ defined in equation (34) and (35) have to be augmented

$$\boldsymbol{Y}_{p+1} = \begin{pmatrix} \boldsymbol{Y}_{p+1,1} & \dots & \boldsymbol{Y}_{p+1,j} \end{pmatrix} \tag{47a}$$

$$\boldsymbol{Z}_p = \begin{pmatrix} \boldsymbol{Z}_{p,1} & \dots & \boldsymbol{Z}_{p,j} \end{pmatrix}. \tag{47b}$$

The data matrices $\boldsymbol{X}_{k+1}$, $\boldsymbol{X}_k$ and $\boldsymbol{U}_k$ in equation (45) are extended in the same way

$$\begin{aligned} \boldsymbol{X}_{k+1} = \begin{pmatrix} \boldsymbol{X}_{p+1,1}(:,2{:}N_1) & \dots & \boldsymbol{X}_{p+1,j}(:,2{:}N_j) \end{pmatrix} \\ \dots \end{aligned} \tag{48}$$

to estimate the system matrices.

In summary, the computational steps of the PBSIDopt algorithm are:

1. Set up the matrices $\boldsymbol{Y}_{p+1}$ and $\boldsymbol{Z}_p$ from equation (47) or equation (34) and (35) respectively,
2. Solve the least squares problem from equation (37),
3. Set up $\boldsymbol{\Gamma}^f \boldsymbol{\mathcal{K}}^p$ from equation (39),
4. Solve the SVD from equation (40),
5. Calculate an estimate of $\boldsymbol{X}_{p+1}$ from equation (41),
6. Solve equation (43) and calculate the innovations from equation (44),
7. Solve equation (46) considering the matrices from equation (48) or (45) respectively.

Because the PBSIDopt method operates in the time domain, the amount of data points to be evaluated is higher than for frequency domain methods. With today's increased computational power, this poses no problem anymore. Like for all time domain methods, the frequency range of interest cannot be specified directly. Filtering the data in a preprocessing step can be used to limit the maximum frequency content in the data. All equations used in the PBSIDopt algorithm are based on linear algebra and no integration is necessary, even if PBSIDopt is a time domain approach. So the method is able to identify unstable systems and can be implemented in a numerically stable and efficient way. Like the ML method, PBSIDopt can handle multiple data sets which is important for rotorcraft system identification.

In contrast to ML, no model structure and thus model states are defined for the PBSIDopt method in advance. PBSIDopt automatically estimates internal states, that are usually unphysical. The system matrices $\boldsymbol{A}$, $\boldsymbol{B}$, and $\boldsymbol{C}$, as appearing in equation (27), are normally fully occupied. Usually, they are not the same as those appearing in equation (1). Rather, PBSIDopt models are comparable to state space models that have been derived from transfer function models, since they only describe the input-output behavior of a system.

3.2. Application to ACT/FHS Flight Data

In this subsection the optimized predictor-based subspace identification method is applied to the identification flight data conducted with DLR's research helicopter ACT/FHS at 60 knots forward flight as described in subsection 2.3. The data consists of eight different flight tests using manual frequency sweeps up to 3 Hz on all control inputs for system identification and eight different 3-2-1-1 step sequences for model validation purposes.

A zero-phase low pass filter with a cutoff frequency of 16.6 Hz is applied to the flight test data and the sampling time is reduced to 24 ms. In this way, high frequency vibrations like the 4/rev oscillation at about 27.5 Hz, are not identified and the computational costs are reduced. The four helicopter controls for longitudinal and lateral cyclic, pedal and collective are used as inputs $\boldsymbol{u}_k$. The velocities u, v and w, the angular rate p, q and r and the attitude angles Φ and Θ are the used outputs $\boldsymbol{y}_k$ to be matched

$$\boldsymbol{u}_k = \begin{pmatrix} \delta_x & \delta_y & \delta_p & \delta_0 \end{pmatrix}^T \tag{49a}$$

$$\boldsymbol{y}_k = \begin{pmatrix} u & v & w & p & q & r & \Phi & \Theta \end{pmatrix}^T. \tag{49b}$$

3.2.1. Influence of Model Order, Future and Past Window Length

As already mentioned in section 3.1, the choice of the future window length f and the past window length p has significant influence on the resulting model accuracy. Even though guidelines for how to chose the past window length p can be found in [11] and [12] as well as the references therein, p has to be large to satisfy equation (36). Furthermore, p should be equal to or greater than the expected model order n to estimate a suitable coefficient matrix Ψ in equation (37) as the basis for the singular value decomposition. The influence of the future window length f is investigated extensively in [12]. It is shown that f highly "depends on the specific experimental conditions" such as the used input signals. So often $p = f$ is fixed and p is chosen to minimize the simulation error, for example in the investigations in [15, 16].

For this paper, a parameter study was conducted to adequately choose the past window length $\boldsymbol{p}_{i_1}$ and the future window length $\boldsymbol{f}_{i_2}$ for the data under investigation. Since the model order is not fixed due to a predefined model structure, for every parameter set $\boldsymbol{p}_{i_1}$ and $\boldsymbol{f}_{i_2}$ 75 models are estimated with the corresponding model order $\boldsymbol{n}_{i_3}$ from 6 to 80.

$$\boldsymbol{p}_{i_1} = \begin{pmatrix} 1 & 2 & 5 & 10 & 20 \dots 250 \end{pmatrix} \tag{50a}$$

$$\boldsymbol{f}_{i_2} = \begin{pmatrix} 1 \dots 5 & 10 & 15 \dots 40 & 50 \dots 100 \end{pmatrix} \tag{50b}$$

$$\boldsymbol{n}_{i_3} = \begin{pmatrix} 6 & 7 \dots 80 \end{pmatrix}. \tag{50c}$$

Since the maximum value of $\boldsymbol{f}_{i_2}$ and $\boldsymbol{n}_{i_3}$ is restricted by the choice of $\boldsymbol{p}_{i_1}$ and $\boldsymbol{f}_{i_2}$ respectively, this parameter study results in 22,942 different models. Using a standard desktop

computer without parallel computing capabilities, this parameter study takes around seven hours including model validation.

The root mean square (RMS) error J_{RMS} is used to quantify model accuracy in the following section. The RMS error between the measurements $\boldsymbol{y}_{\mathrm{m}}$ and the simulated model outputs $\boldsymbol{y}$ is defined as

$$J_{\mathrm{RMS}} = \sqrt{\frac{1}{n_y N} \sum_{k=1}^{N} \left(\boldsymbol{y}_{\mathrm{m},k} - \boldsymbol{y}_k\right)^T \left(\boldsymbol{y}_{\mathrm{m},k} - \boldsymbol{y}_k\right)} \tag{51}$$

with the number of data samples N and the number of outputs n_y. According to [1] a root mean square error of

$$J_{\mathrm{RMS}} \leq 1.0 \text{ to } 2.0 \tag{52}$$

indicates a good overall model accuracy for coupled helicopter models using typical time domain validation maneuvers like 3-2-1-1 sequences, if ft/s, deg/s and deg are used as output units.

In figure 2, the smallest RMS errors of the identified ACT/FHS models are shown as a function of the parameters p and f. Low RMS errors are drawn in light yellow, larger ones in red to black. For very small $f \leq 5$, the models suffer from large RMS errors, because the model order is limited to $n_u n_y f$ and thus is small. Suitable identification parameter sets can be found for $f \approx 20$ and $f \geq 45$ if $p > 150$. For the flight test data under consideration, large values for f and p seems to be a good choice for accurate results, but increase the necessary computational time significantly. Setting $p = f$ does not result in the lowest RMS errors possible for this experimental setup.

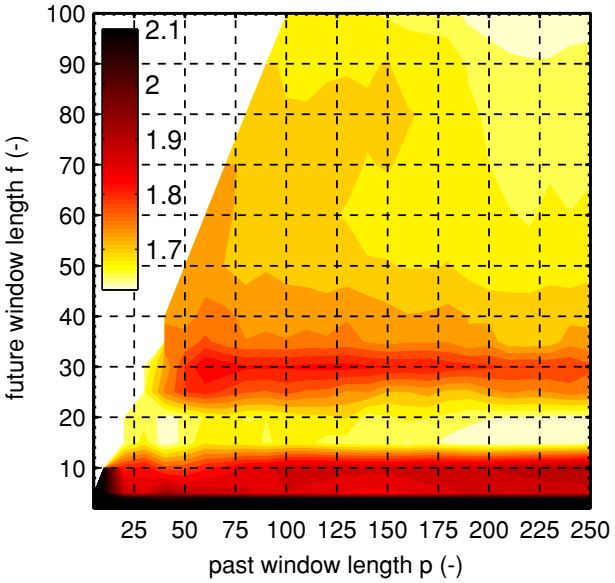

Figure 2: Minimal RMS errors of identified ACT/FHS models as a function of past and future window length

Even if figure 2 can be used to chose the identified model with the smallest RMS error, it does not give information about the other models identified in the parameter study. To analyze the RMS error distribution as a function of the model order, the box-plots in figure 3 (on the next page) are used. In figure 3, the whiskers mark the maximum and minimum RMS values of the identified models with a defined order, if there are no RMS values larger or smaller than four times the interquartile range. Otherwise the whiskers mark the largest and smallest existent RMS error up to four times the interquartile range and outliers are depicted as additional circles. It can be seen, that the RMS error distribution converges to small error values with higher model order n. Nevertheless the identified model with the lowest RMS error has $n = 34$ which can be seen at the lowest whisker in figure 3. As expected, low order models do not cover the highly coupled helicopter dynamics sufficiently. Since the majority of the identified models with $n > 20$ have small RMS errors and a narrow error distribution, a huge set of appropriate models is identified using the PBSIDopt method. (The RMS errors for $n = 51$ to $n = 80$ are not shown in the figure.)

3.2.2. Model Order Selection

As mentioned in section 3.1, the neglect of smaller singular values in the predictor sequence reconstruction in equation (41) can be interpreted as a model reduction step. Often the singular values are investigated in this step to select an appropriate model order [14]. In figure 4, the singular values are shown for the parameter set $f = 100$ and $p = 220$ (as this set results in the lowest RMS error model with model order $n = 34$).

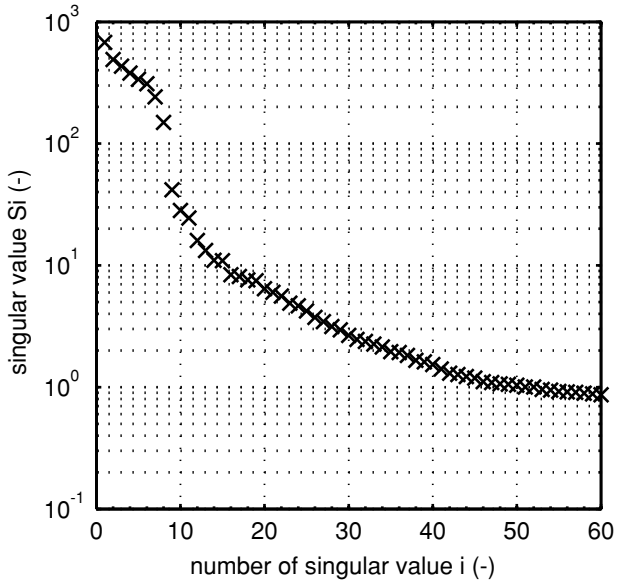

Figure 4: Singular value plot for model order estimation

A clear gap between the 8th and 9th singular value can be observed, but a model order of $n = 8$ is not sufficient to achieve a good model accuracy (see figure 3). After $i = 16$ the singular values decrease slower than before. This cor-

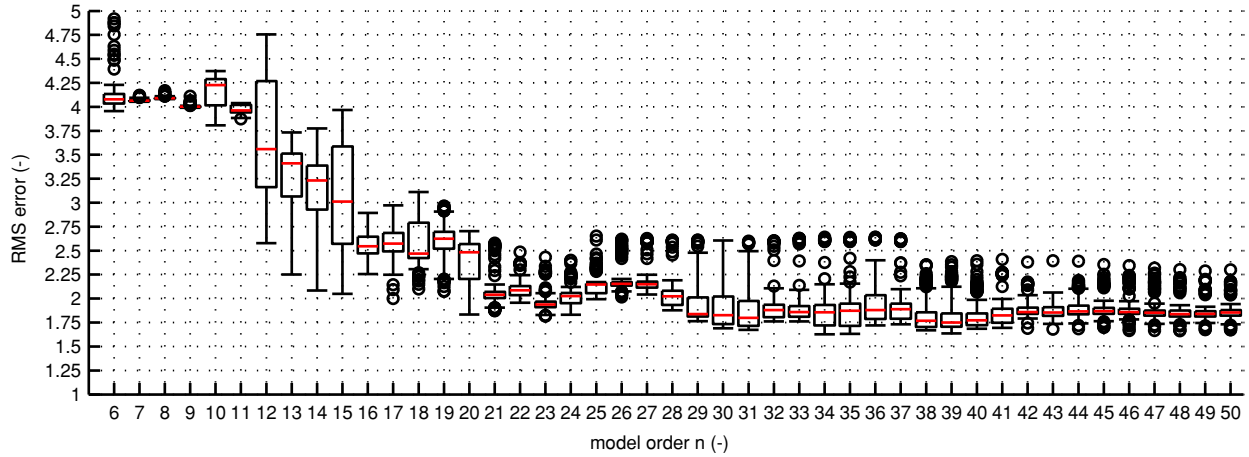

Figure 3: RMS error distribution of identified ACT/FHS models as a function of model order n ($f \geq 10$)

respond to figure 3, in which the minimal RMS error reaches a value of 2.25 for $n = 16$. Also note that the singular values do not converge to zero, since there is measurement noise.

Thus, the investigation of the singular values in figure 4 can be helpful to select a minimal model order to start the system identification process, but a clear decision on what model order is sufficient or even best for the predictor sequence estimation cannot be arrived at. So the model order selection should be based on the validation results and not on the singular values, even if the chosen model order might be high.

For further investigation, two different models are selected: A 15th order model ($f = 15$, $p = 30$, $J_{\mathrm{RMS}} = 2.06$) is investigated without any further processing steps, as this corresponds to the ML model with 15 states. In addition, the 34th order model with the lowest RMS value is chosen ($f = 100$, $p = 220$, $J_{\mathrm{RMS}} = 1.61$). This model is reduced to an appropriate order in the following subsection.

3.2.3. Model Reduction

Depending on the intended usage of a low order model, only a certain frequency range has to be matched appropriately. For ACT/FHS control applications a frequency range from 0.5 rad/s to 20 rad/s is used. Most of the relevant flight dynamics are covered in this frequency range and higher dynamics cannot not be compensated through classical feedback controllers. Slower dynamics can be compensated easily, so their representation can be simplified for control issues, but they need to be correct for simulation usage. During the Maximum Likelihood frequency domain system identification presented in section 2, these frequency limits can be considered directly, but this is not possible in a time domain approach like the PBSIDopt algorithm.

Model reduction techniques provide the possibility to reduce model complexity and to account for the frequency range of interest. In this paper, the identified 34th order model $\boldsymbol{G}(s)$ is decomposed into its slow and high frequency parts using a method based on [22]

$$\boldsymbol{G}(s) = \boldsymbol{G}_{\mathrm{slow}}(s) + \boldsymbol{G}_{\mathrm{fast}}(s). \tag{53}$$

The fast dynamics $\boldsymbol{G}_{\mathrm{fast}}(s)$ are neglected afterwards, whereas the remaining slow frequency dynamics $\boldsymbol{G}_{\mathrm{slow}}$ are used as a reduced model.

The identified 34th order model is reduced by removing the dynamics faster than 20 rad/s (to match the frequency range of interest used in section 2). In this way the 34th order model is scaled down to a 18th order model. Figure 5 compares the original and reduced model using the example of collective input δ_0 to heave motion w. The first low-damped oscillation at about 34 rad/s that is omitted in the model reduction step can be attributed to the tail boom structural mode and coning. Further high order effects of the 34th order model are related to physical effect, used digital filters or numerical effects in the system identification process. These undesirable numerical effects increase with higher system order and should always be removed from the model.

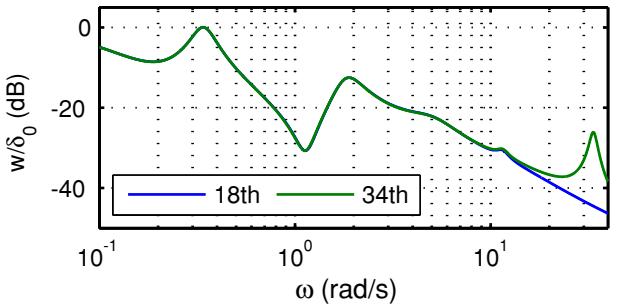

Figure 5: Original and reduced order ACT/FHS models

The identified 15th order model described in section 3.2.2 and the 18th order model are compared to the measured

frequency response in figure 6 for lateral inputs δ_y to the roll rate p and pitch rate q. Both models are matching the roll rate p accurately for frequencies $\omega > 0.4\,\mathrm{rad/s}$. The pitch rate dynamics show larger variations of both models to each other. The 18th order model is much more accurate over the whole frequency range of interest. The regressive lead-lag dynamics at about 12 rad/s are only identified in the 18th order model, but not in the 15th order PBSIDopt model (in contrast to the 15th order ML model). Thus, the reduction of a high order model results in smaller errors compared to estimating a low order model directly (model reduction vs. under modeling [23]). Due to the deficiencies of the 15th order model, only the 18th order model is investigated further in the following section.

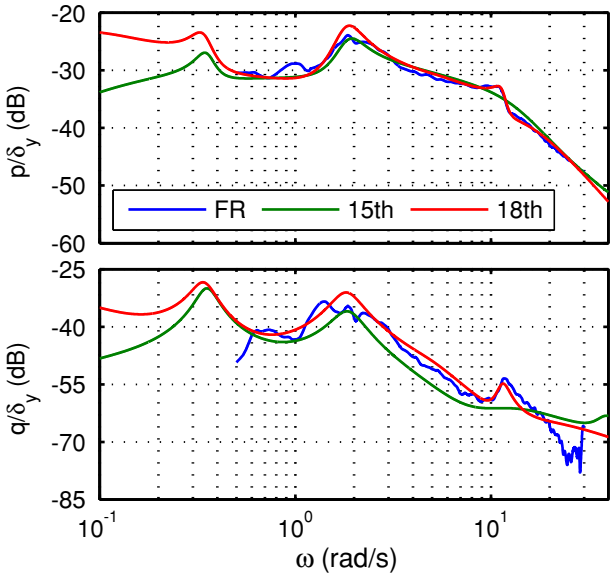

Figure 6: Comparison of measured frequency response (FR) with 15th and 18th order PBSIDopt model

4. Comparison of Frequency Domain and PBSIDopt Identified ACT/FHS Models

Rotorcraft model validation in time domain is usually performed using doublet or multi-step inputs. As mentioned in section 3.2, the (overall) RMS error is used to quantify the models' accuracy and chose the best PBSIDopt model for further investigation. The RMS errors from the eight different validation maneuvers are listed in table 1. The first row marks the validation maneuver, where $+\delta_x$ is a 3-2-1-1 step sequence on the δ_x control in positive direction. The second and third row contain the corresponding RMS errors from the ML model and the PBSIDopt model respectively. The overall RMS errors of both models are shown in the last column.

Regarding the results in table 1, the longitudinal maneuvers of the ML model are rated poorly. The large RMS errors are mainly caused by low frequency deviations in the forward velocity u, the roll rate p and the pitch rate q. In the left part

	$+\delta_x$	$-\delta_x$	$+\delta_y$	$-\delta_y$	$+\delta_p$	$-\delta_p$	$+\delta_0$	$-\delta_0$	J_{RMS}
ML	4.4	2.4	1.2	1.6	1.8	1.9	2.3	3.4	2.6
PB	2.1	1.5	1.3	1.2	1.8	1.9	1.1	1.9	1.6

Table 1: RMS errors of Maximum Likelihood (ML) and PBSIDopt (PB) models for different validation maneuvers

of figure 7, this effect is clearly visible in the time domain comparison of the $-\delta_x$ maneuver. These deviations are not weighted in the ML optimization step, since frequencies below 0.5 rad/s are not considered. The yaw rate r shows nonlinear effects due to the fenestron tail rotor, which cannot be matched by both methods, since they provide linear models only.

In the frequency domain comparison in figure 8, both models match the measured amplitude responses very well for mid and high frequencies from δ_x to heave motion w, roll rate p and pitch rate q. The frequency sweep maneuvers that are used to calculate the frequency responses in blue ("FR") are the same that are used for both identification methods in section 2 and 3. Some variations are observed for the forward and lateral velocities u and v and the yaw rate r, nevertheless both methods provide good results in the frequency range of interest.

Both methods accurately model the responses to lateral cyclic inputs δ_y regarding the corresponding RMS values in table 1. The PBSIDopt model does not show much better results, even if the amplitude responses are captured more precisely from lateral cyclic to the velocities u and w shown in figure 9. A time domain comparison of the positive lateral cyclic maneuver $+\delta_y$ is shown in the right part of figure 7. Here, the ML model can be considered as being more accurate for the velocity u, nevertheless these are low frequency deviations. The identified roll rate p shows better results for the PBSIDopt model, but the ML model is also very accurate. The regressive lead-lag resonance can be clearly seen at about 12 rad/s in the roll and pitch rates in figure 9. While these dynamics are covered by one complex pole in the PBSIDopt model only, the ML frequency domain model needs two complex poles with the same dynamics to cover these effects due to the predefined model structure, see subsection 2.2.3. Since the regressive lead-lag resonance is clearly visible in the input-output relations of the helicopter, the associated dynamics of PBSIDopt model can be attributed to a physical phenomenon in this case. Nevertheless, internal physical relations are usually difficult to be interpreted in the PBSIDopt model. The overall performance from lateral cyclic inputs of both models is very good.

The responses to pedal inputs (figure 10) are captured very well by both models for frequencies around 1 rad/s. Large differences between the models can be found in the representation of the forward velocity u for low and high fre-

quencies, but the RMS errors of both models are rated as good. The PBSIDopt model includes additional regressive lead-lag dynamics also for pedal inputs, as can be seen in the transfer functions for roll rate p and pitch rate q. Due to the model structure of the ML model, where the lead-lag motion is only excited by cyclic control inputs, these couplings are not included in the ML model. Furthermore, the model identified by the ML method in frequency domain, seems to suffer from an underestimated yaw rate amplitude for $\omega > 3\,\mathrm{rad/s}$, but there is no need for the extension of the ML model with further dynamics.

The largest differences between the models can be found for collective inputs δ_0 shown in figure 11. The deficiencies of the ML frequency domain model for collective inputs are caused by the missing engine dynamics and can also clearly be seen in the high RMS errors for the validation maneuvers in table 1. The ML model has also some deficiencies describing couplings from collective to lateral velocity v, roll rate p and yaw rate r. These deficiencies have already been investigated in [7] and [8]. The significant dynamics of the PBSIDopt model for collective inputs can provide useful information to enhance the ML model structure for an iterative model enhancement, since the PBSIDopt model covers three more states (or five concerning the four regressive lead-lag states as two states only). The regressive lead-lag dynamics at 12 rad/s are highly excited by collective inputs, which is not included in the ML model. The modeling approach described in subsection 2.2.3 might be improved using these PBSIDopt model results. The on-axis response from δ_0 to heave motion w is covered more accurately in the ML model for higher frequencies. High frequency dynamics for $\omega \approx 34\,\mathrm{rad/s}$ are not covered by both models due to the applied frequency limits.

The overall RMS error of the PBSIDopt model can be considered as good: $J_{\mathrm{RMS}} < 2$. Missing cross-couplings and engine dynamics result in $J_{\mathrm{RMS}} > 2$ for the ML model. Nevertheless, this model shows very good results for lateral cyclic and pedal inputs and has a model order of 15 only (compared to 18th order PBSIDopt model). Since the ML model structure is motivated physically, it only contains effects, which are accounted for in the defined model structure. Including additional states describing the engine dynamics in the ML model, might cover some of the missing effects and reduce the RMS error to the PBSIDopt model level. For further investigation, the PBSIDopt model will be used to enhance the ML model with the missing dynamics for collective inputs mainly.

5. Conclusions and Outlook

The PBSIDopt method has successfully been applied to flight test data of the ACT/FHS research helicopter and models that are accurate over a broad frequency range have been identified. The results have been compared to a model identified by the classical ML frequency domain output error method.

The ML method needs a predefined model structure, which leads to physically interpretable models, but all important dynamic effects have to be accounted for in the model structure. The presented ACT/FHS model identified with the ML method does not yet contain engine dynamics. Therefore, this model still has deficiencies for collective inputs. Furthermore, the regressive lead-lag dynamics are only excited by cyclic inputs. As the ML method works in frequency domain, the computational costs are low and models of unstable systems can be estimated. Nevertheless, good initial values for the optimization problem are needed, especially for rotorcraft applications.

The PBSIDopt method estimates an input-output state space model with fully occupied system matrices $\boldsymbol{A}$, $\boldsymbol{B}$ and $\boldsymbol{C}$. The physical interpretation of the models is hard, since the model states cannot be defined beforehand. Compared to the ML model, the fidelity of the PBSIDopt model is higher, because single dynamic effects do not have to be modeled explicitly, the model contains three more states and is fully coupled. Just like the ML method, the PBSIDopt method is able to estimate models from unstable processes and is numerical stable. Nevertheless, the computational costs and the resulting model order can be high. A model reduction step is necessary to gain models which cover the frequency range of interest only.

For further evaluation, the PBSIDopt method can be considered as a useful addition to the Maximum Likelihood method in frequency domain. The PBSIDopt model can give useful information about missing dynamical effects which can modeled linearly and the needed model order to cover them. The missing engine dynamics of the ACT/FHS ML model will be analyzed in a future work, the couplings of the regressive lead-lag dynamics might be improved using the PBSIDopt model as reference.

The application of the identified PBSIDopt models to the ACT/FHS model-based control system, i.e. for feedforward controller design, will be investigated, but further requirements like invertibility of the model have to be ensured. Since experiment design for rotorcraft system identification still is very complicated, the dedicated flight test design should be analyzed and optimized with respect to the ML and PBSIDopt method in the future.

References

[1] M. B. Tischler and R. K. Remple, *Aircraft and Rotorcraft System Identification: Engineering Methods with Flight-Test Examples*. American Institute of Aeronautics and Astronautics, Inc., Reston, Virginia, second ed., 2012.

[2] R. Lantzsch, S. Greiser, J. Wolfram, J. Wartmann, M. Müllhäuser, T. Lüken, H.-U. Döhler, and N. Peinecke, "ALLFlight: A Full Scale Pilot Assistance Test Environment," in *American Helicopter Society 68th Annual Forum*, (Ft. Worth, Texas, USA), 2012.

[3] J. Kaletka, H. Kurscheid, and U. Butter, "FHS, the New Research Helicopter: Ready for Service," *Aerospace Science and Technology*, vol. 9, pp. 456–467, July 2005.

[4] S. Seher-Weiss and W. von Grünhagen, "EC135 System Identification for Model Following Control and Turbulence Modeling," *Proceedings of the 1st CEAS European Air and Space Conference 2007*, pp. 2439–2447, 2007.

[5] S. Seher-Weiss and W. von Grünhagen, "Development of EC 135 Turbulence Models via System Identification," *Aerospace Science and Technology*, 2011.

[6] S. Seher-Weiss and W. von Grünhagen, "Comparing Explicit and Implicit Modeling of Rotor Flapping Dynamics for the EC135," in *Deutscher Luft- und Raumfahrtkongress*, (Berlin, Germany), 2012.

[7] J. Wartmann, "Model Validation and Analysis Using Feedforward Control Flight Test Data," in *Deutscher Luft- und Raumfahrtkongress*, (Berlin, Germany), 2012.

[8] S. Greiser and W. von Grünhagen, "Analysis of Model Uncertainties Using Inverse Simulation," in *American Helicopter Society 69th Annual Forum*, (Phoenix, Arizona, USA), 2013.

[9] A. Chiuso and G. Picci, "Consistency analysis of some closed-loop subspace identification methods," *Automatica*, vol. 41, pp. 377–391, Mar. 2005.

[10] A. Chiuso, "On the relation between CCA and predictor-based subspace identification," *Proceedings of the 44th IEEE Conference on Decision and Control*, pp. 4976–4982, 2005.

[11] A. Chiuso, "The role of vector autoregressive modeling in predictor-based subspace identification," *Automatica*, vol. 43, pp. 1034–1048, June 2007.

[12] A. Chiuso, "On the Asymptotic Properties of Closed-Loop CCA-Type Subspace Algorithms: Equivalence Results and Role of the Future Horizon," *IEEE Transactions on Automatic Control*, vol. 55, no. 3, pp. 634–649, 2010.

[13] P. Li, I. Postlethwaite, and M. C. Turner, "Subspace-based System Identification for Helicopter Dynamic Modelling," in *American Helicopter Society 63rd Annual Forum*, (Virginia Beach, Virginia, USA), 2007.

[14] P. Li and I. Postlethwaite, "Subspace and Bootstrap-Based Techniques for Helicopter Model Identification," *Journal of the American Helicopter Society*, vol. 56, no. 1, 2011.

[15] M. Bergamasco and M. Lovera, "Continuous-Time Predictor-Based Subspace Identification For Helicopter Dynamics," in *European Rotorcraft Forum*, (Milano, Italy), 2011.

[16] M. Sguanci, M. Bergamasco, and M. Lovera, "Continuous-Time Model Identification for Rotorcraft Dynamics," in *16th IFAC Symposium on System Identification*, (Brussels, Belgium), 2012.

[17] M. Verhaegen and A. Varga, "Some Experience with the MOESP Class of Subspace Model Identification Methods in identifying the BO105 Helicopter," tech. rep., German Aerospace Research Establishment, Institute for Robotics and System Dynamics, 1994.

[18] M. Marchand and K.-H. Fu, "Frequency Domain Parameter Estimation of Aeronautical Systems with and without Time Delay," in *Proc. of the 7th IFAC Symposium on Identification and System Parameter Estimation*, (York, UK), pp. 669–674, 1985.

[19] J. A. Schroeder, M. B. Tischler, D. C. Watson, and M. M. Eshow, "Identification and Simulation Evaluation of a Combat Helicopter in Hover," *Journal of Guidance, Control and Dynamics*, vol. 18, no. 1, 1995.

[20] S. Greiser and S. Seher-Weiss, "A Contribution to the Development of A Fullflight Quasi-Nonlinear Helicopter Simulation," in *Deutscher Luft- und Raumfahrtkongress 2012*, (Berlin, Germany), 2012.

[21] L. Ljung, *System Identification: Theory for the User*. P T R Prentice Hall, Englewood Cliffs, New Jersey, 1987.

[22] M. G. Safonov and R. Y. Chiang, "A Schur Method for Balanced-Truncation Model Reduction," *IEEE Transactions on Automatic Control*, vol. 34, no. 7, 1989.

[23] F. Tjärnström, "Variance analysis of L2 model reduction when undermodeling - the output error case," *Automatica*, vol. 39, Oct. 2003.

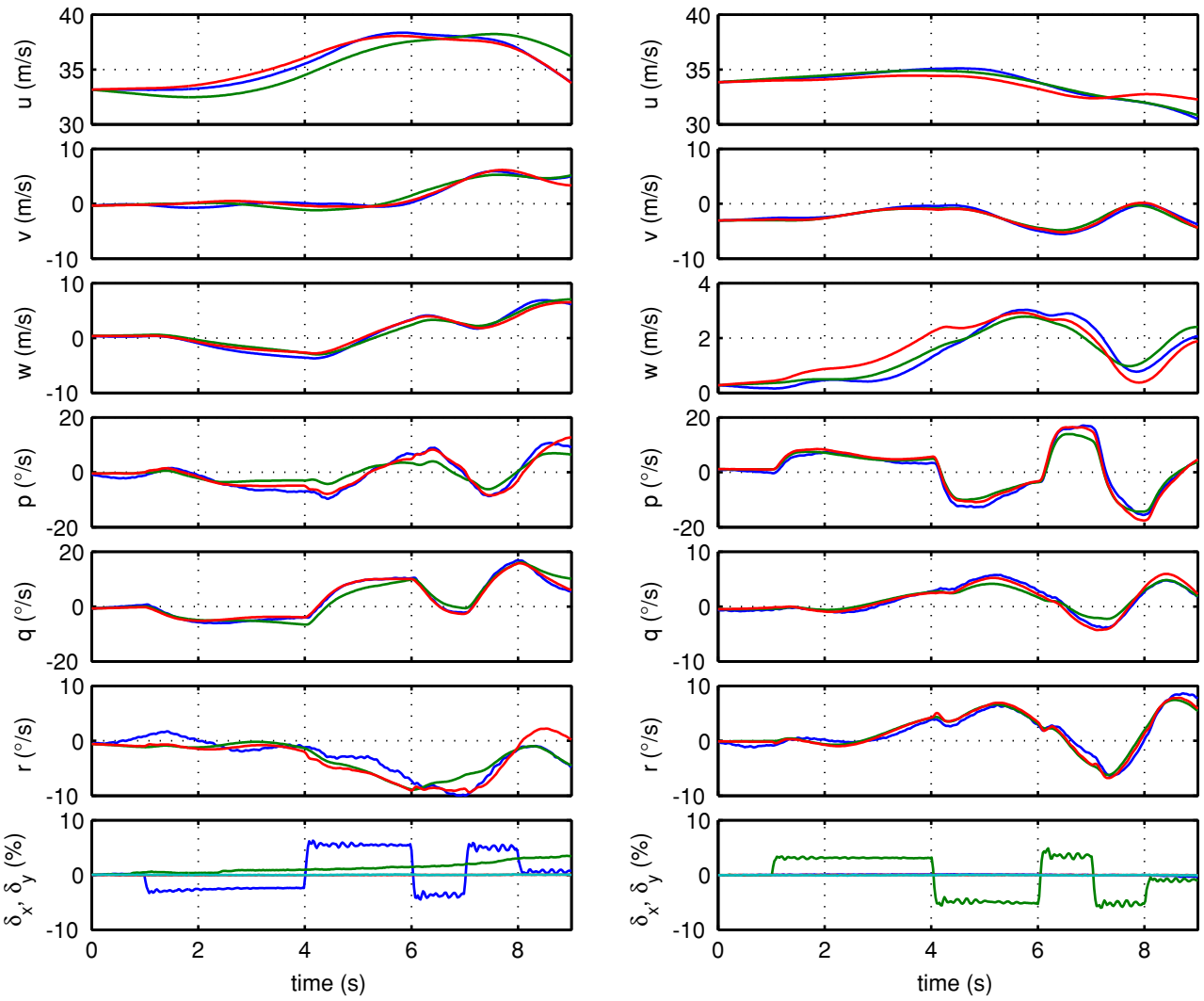

Figure 7: Time domain responses of ACT/FHS models from $-\delta_x$ (left) and δ_y (right) inputs at 60 knots forward flight (blue - measured response, green - ML model, red - PBSIDopt model)

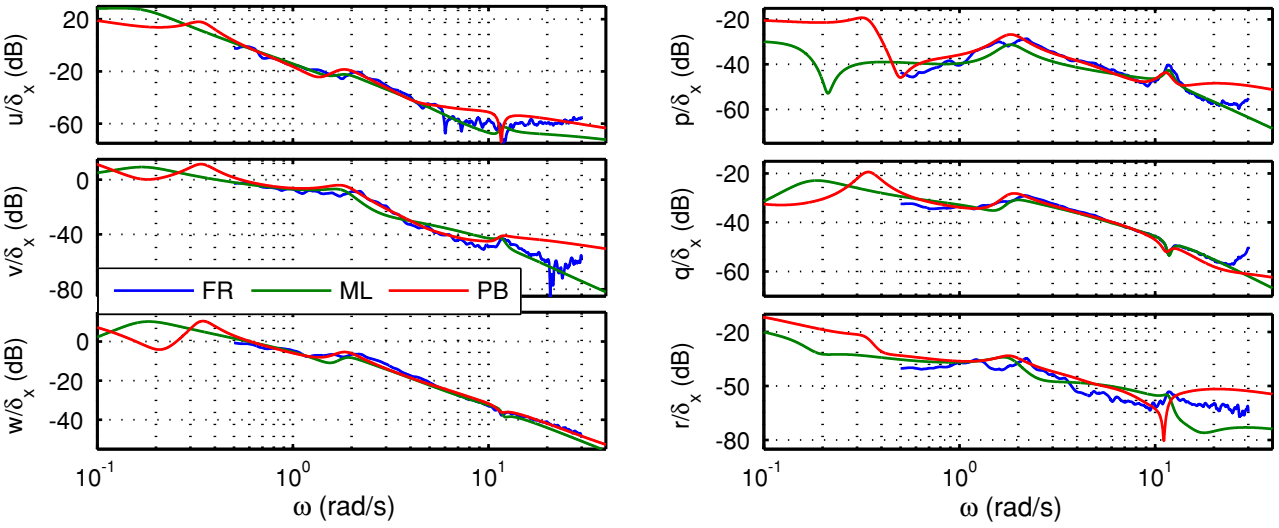

Figure 8: Amplitude responses of ACT/FHS models from longitudinal cyclic inputs at 60 knots forward flight (FR/blue - measured frequency response, ML/green - Maximum Likelihood model, PB/red - PBSIDopt model)

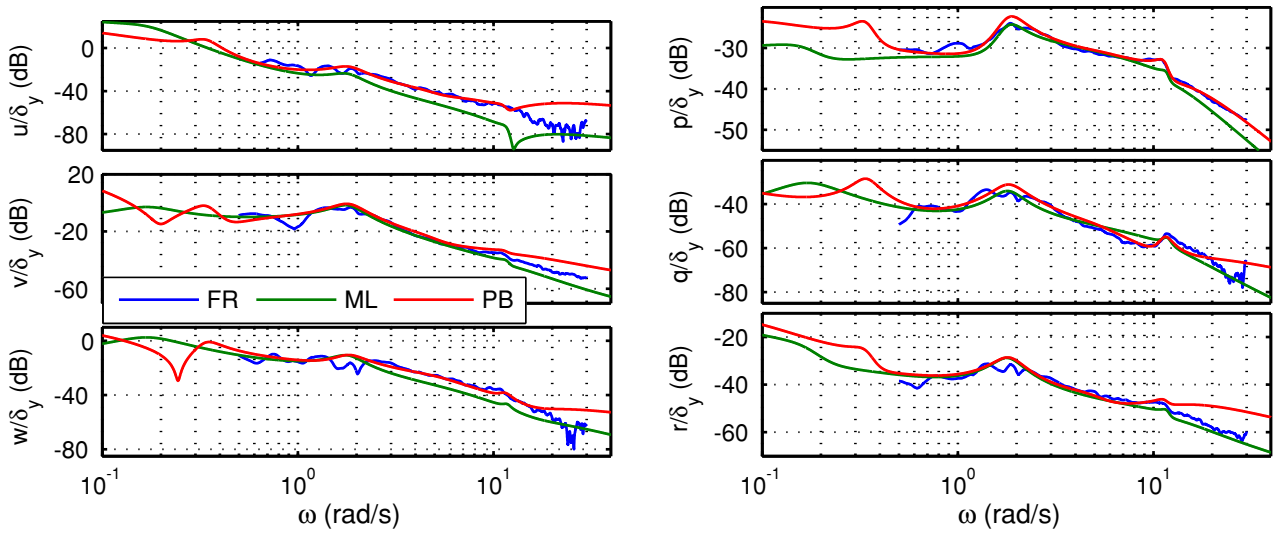

Figure 9: Amplitude responses of ACT/FHS models from lateral cyclic inputs at 60 knots forward flight
(FR/blue - measured frequency response, ML/green - Maximum Likelihood model, PB/red - PBSIDopt model)

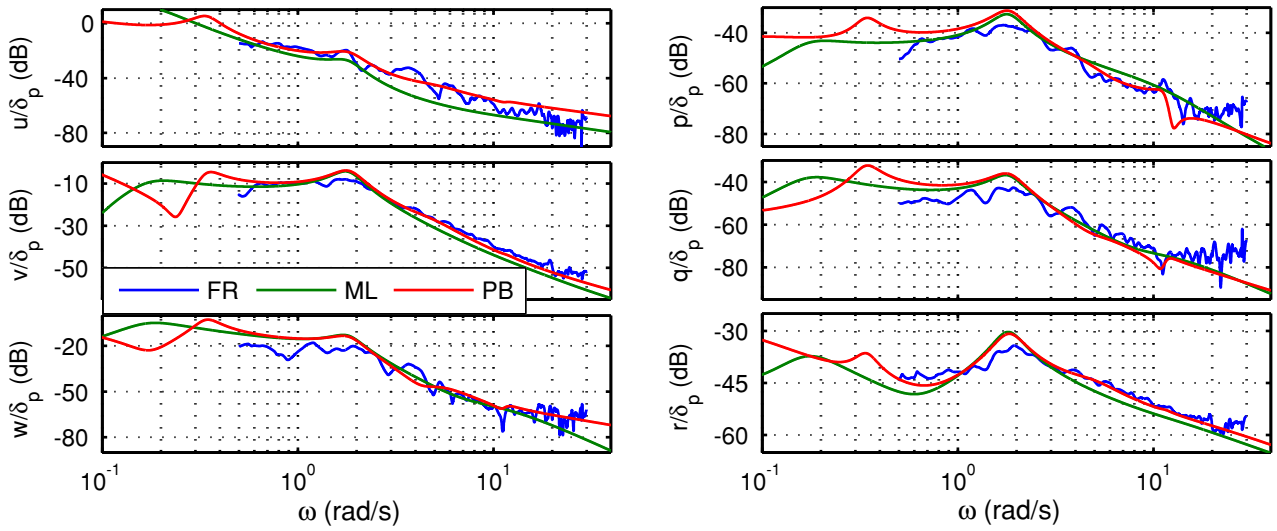

Figure 10: Amplitude responses of ACT/FHS models from pedal inputs at 60 knots forward flight

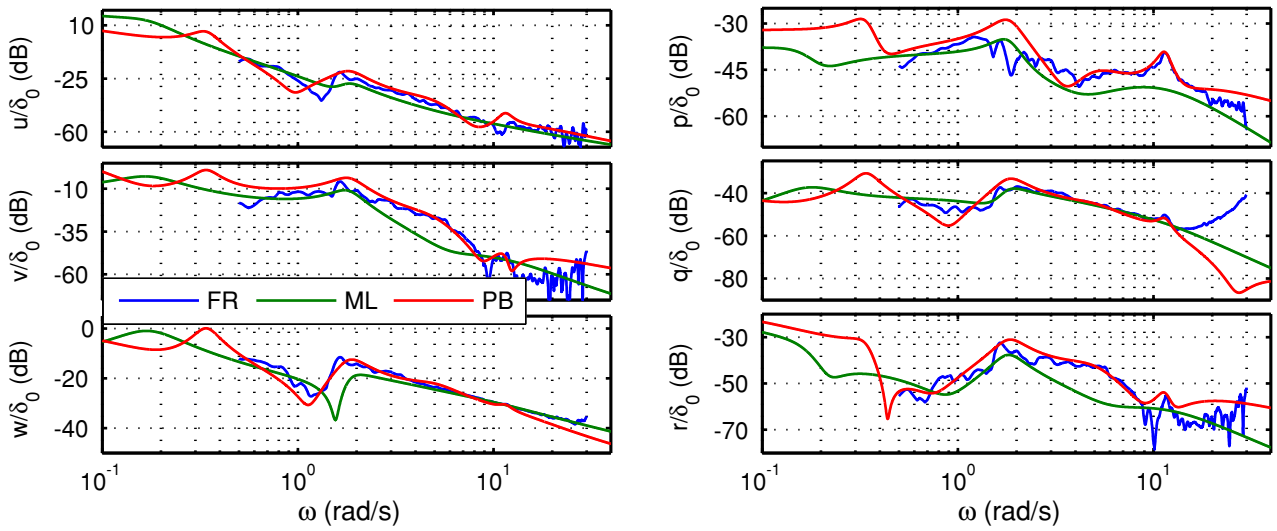

Figure 11: Amplitude responses of ACT/FHS models from collective inputs at 60 knots forward flight